Chinese Chemical Letters 31 (2020) 2003–2006

Contents lists available at ScienceDirect

Chinese Chemical Letters

journal homepage: www.elsevier.com/locate/cclet

Communication

Yolk-shell structured Fe@void@mesoporous silica with high magnetization for activating peroxymonosulfate

Bingqian Xu[a], Wan Jiang[a], Lianjun Wang[a], Binota Thokchom[b], Pengpeng Qiu[a,*], Wei Luo[a,*]

[a] State Key Laboratory for Modification of Chemical Fibers and Polymer Materials, College of Materials Science and Engineering, Donghua University, Shanghai 201620, China
[b] Indian Institute of Technology Guwahati, Guwahati 781039, India

ARTICLE INFO

Article history:
Received 20 November 2019
Received in revised form 19 December 2019
Accepted 26 December 2019
Available online 26 December 2019

Keywords:
Yolk-shell
Magnetic mesoporous silica
Fenton-like process
PMS activation
Tetracyclines

ABSTRACT

Sulfate radical anion ($SO_4^{\bullet-}$) based Fenton-like reaction have recently received a large quantity of attention owing to their strong oxidative capacity and high selectivity toward organic pollutants. However, the development of a high-efficient catalyst for activation of peroxymonosulfate (PMS) with a fast separation is still challengeable. Herein, magnetic mesoporous silica composites with a yolk-shell structure (Fe@void@mSiO_2) have been prepared *via* a successive coating strategy, followed by a high-temperature *in-situ* treatment and demonstrated as a high-efficient and fast magnetic separable catalyst for the activation of PMS. The resultant material possesses a well-defined yolk–shell structure with high specific surface area (~495.0 m^2/g), uniform pore size (~6.9 nm) and super large magnetic susceptibility (~105 emu/g). Owing to the unique properties, the material possesses an excellent degradation activity for tetracyclines (TC), which is much higher than the commercialized Zero Valent Iron (ZVI) nanoparticles. Additionally, the catalyst is able to work over a broad pH range and be quickly recycled by using an external magnetic field. This research provides a promising strategy for the synthesis and design of multifunctional catalyst for the Fenton-like process.

Tetracycline (TC), as a typical broad-spectrum antibiotic, has been widely employed in veterinary, agricultural and humanic therapeutics. However, only little amount of TC can be metabolized by humans and animals owing to its chemical structure and recalcitrance to biological degradation, which results in the massive release of its residues into the environment, affecting the ecosystem. Therefore, the development of an alternative technology to efficiently remove TC is urgent [1–3].

Based on hydrogen peroxide (H_2O_2) and ferrous ions, the Fenton process has recently garnered tremendous attention as an efficient approach to degrade organic pollutants *via* the hydroxyl radical ($^{\bullet}OH$) oxidation [4–9]. Whereas, narrow work pH range and the low utilization rate of H_2O_2 significantly limit its applications in actual water treatment [10,11]. As an alternative, through the activation of peroxymonosulfate (PMS), the sulfate radical ($SO_4^{\bullet-}$) based Fenton-like system [12,13] has recently been widely investigated due to it not only shows higher oxidation potentials ($SO_4^{\bullet-}$ (2.5–3.1 V) > $^{\bullet}OH$ (1.8–2.7 V)) but also works in wide pH ranges [14,15]. Till now, various strategies such as base, heat, ultrasound transition metals and ultraviolet (UV) have been adopted to active PMS [16–18]. Among them, the utilization of transition-metal ions such as Mn^{2+}, Co^{2+} and Cu^{2+}, are of great significance owing to its high efficiency and abundant resources [19–21]. But during application such as in a slurry operating system, they are especially arduous to be separated and regenerated. Separation can be enhanced in the form of particles, but the catalytic efficiency was reduced owing to the decrease of active sites. Therefore, the development of a catalyst for degradation of TC and activation of PMS with simultaneous facile separation and high efficiency is desirable.

Recently, yolk-shell structured mesoporous materials have shown great promise in diverse applications such as drug delivery [22,23], sensors [24–26], energy storage [27], confined catalysis [28–30] and adsorption [31,32] due to the unique structure of inner active core, middle void spaces, and outer mesoporous shells. Among them, the Fe_3O_4@void@mesoporous SiO_2 (mSiO_2) nanostructures are of great interest due to their superior properties such as strong magnetic separation ability, outstanding

* Corresponding authors.
E-mail addresses: qiupengpeng@dhu.edu.cn (P. Qiu), wluo@dhu.edu.cn (W. Luo)

https://doi.org/10.1016/j.cclet.2019.12.035

biocompatibility, abundant catalytic sites, high specific surface area and multi-functional interfaces [33–35]. However, the small magnetization of the resultant materials still hinders their practical applications. The utilization of Fe, Co, Ni or alloys metal cores [36,37] may resolve this problem, but they are easy to suffer from aggregation and the surface of them are hard to be functionalized during the synthesis, which are undesirable for the further coating. Consequently, the development of a facile method to synthesize Fe@void@mesoporous SiO_2 ($mSiO_2$) is much desired.

Herein, we have developed a facile strategy to prepare magnetic yolk-shell structured mesoporous silica nanospheres (Fe@void@$mSiO_2$). The synthesis involved a successive coating strategy, followed by a high-temperature *in-situ* transform of Fe_3O_4 to Fe nanoparticles. The introduction of a middle carbon layer between mesoporous silica shell and Fe_3O_4 core is to *in-situ* reduce Fe_3O_4 to Fe and generate void space during the carbonization process. The resultant materials show a well-defined yolk–shell structure with high specific surface area (495.0 m^2/g), uniform pore size (6.9 nm) and super large magnetic susceptibility (105 emu/g). Finally, dedicated to the activation of PMS, the material used as a catalyst shows an excellent degradation activity for TC in a wide pH range. Moreover, the catalyst is able to be fast recycled *via* applying an external magnetic field, which holds a great promise in the practical application.

All chemicals without further purification were used as received. Millipore water was suitable for all experiments. $FeCl_3{\cdot}6H_2O$, PMS ($KHSO_5{\cdot}0.5KHSO_4{\cdot}0.5K_2SO_4$), tetraethyl orthosilicate (TEOS), ethanol, methanol, cyclohexane, trisodium citrate, ammonia solution (28 wt%), ethylene glycol, sodium acetate, hexadecyl trimethyl ammonium bromide and TCL were purchased from Shanghai Chemical Corp.

Referring to previous work, a solvothermal method is adopted to the preparation of superparamagnetic Fe_3O_4 nanoparticles [38–40]. In brief, sodium acetate (NaAc, 6.0 g), trisodium citrate (1.3 g) and $FeCl_3{\cdot}6H_2O$ (3.25 g) were added to ethylene glycol (80 mL) with stirring and dissolve. The mixture stirred strongly at room temperature for 1 h was poured into a stainless-steel autoclave lined with Teflon and 100 mL volume. The autoclave was kept for 10 h at 200 °C, and slowly cooled to room temperature follow. The products obtained were washed for 3 times with EtOH and deionized water, separately, and then dispersed in EtOH (45 mL) for the next step.

Fe_3O_4 ethanol dispersion (3 mL) was sonicated and dissolved in a mixed solution of deionized water (10 mL) and EtOH (20 mL). Subsequently, formaldehyde (0.10 g, 37 wt%), resorcinol (0.10 g, 0.09 mmol/L) and ammonia solution (0.50 g, 28 wt%) were continuously added. Formaldehyde polymerization of formaldehyde and resorcinol on Fe_3O_4 particles occurred in the mixed dispersion after mechanical stirring for 10 h at 45 °C. *Via* washed with EtOH and deionized water as well as magnet for three times, separately, the core-shell Fe_3O_4@RF microspheres were obtained.

A mixed solution containing concentrated aqueous ammonia (0.80 mL, 28 wt%), deionized water (80 mL) and CTAB [41,42] (0.50 g, 1.3 mmol) was prepared, and then the Fe_3O_4@RF nanoparticles obtained above were dispersed in them by sonication. Subsequently, a two-phase system was formed with the supplement of cyclohexane (20 mL). Then, TEOS (0.5 mL) was added into the oil phase, and the reaction was maintained at 45 °C with slow agitation (100 rpm) for 6 h [43]. The product collected by the magnet was washed three times with EtOH and water, respectively. Finally, the microspheres were obtained by calcination in N_2 atmosphere at 850 °C.

Transmission electron microscopy (TEM) images was taken on a JEOL 2011 microscope (Japan). Prior to TEM measurements, the sample was dispersed in EtOH and dropped on a holey carbon film on a Cu grid. Vibrating Sample Magnetometer (EV9, Microsense, Japan) was used to measure the magnetization. XRD patterns were obtained on a Bruker D8X-ray diffractometer with Ni-filtered Cu Kα radiation (40 kV, 40 mA). Nitrogen sorption isotherms were measured with a Micromeritics Tristar 3020 analyzer (USA) at 77 K. Before the measurements, the samples were degassed in a vacuum at 180 °C for 6 h. The specific surface areas (S_{BET}) was calculated using adsorption data in the relative pressure range P/P_0 = 0.05–0.3 based on Brunauer-Emmett-Teller (BET) method. The Barrett-Joyner-Halenda (BJH) model was applied to estimate the pore size distributions from the adsorption branches of the isotherms. The total pore volumes were calculated from the adsorbed amount at the relative pressure P/P_0 = 0.995.

Catalyst (0.05 g) and aqueous suspensions (100 mL) of TC (10 mg/L) were added into a double-layered cylindrical reactor (100 mL in capacity). The utilization of a water jacket maintains the temperature of the solution at 20 °C. The mixture was mechanically stirred for 30 min in dark before the addition of PMS (0.18 g) to achieve an adsorption/desorption equilibrium between the contaminants and the catalyst. Then, the suspension (0.5 mL) was removed through the utilization of a 1 mL syringe at given time intervals and was filtered *via* a membrane with a pore size of 0.45 μm. Moreover, methanol (2 mL) was added to the sample above to terminate the reaction. The mixed solution was analyzed by recording the variations in the maximum absorption band (405 nm) using a Thermo Spectronic UV 500 UV–vis spectrometer.

Fig. 1 shows illustration of the formation of yolk-shell structured Fe@void@$mSiO_2$ composites by a facile and straightforward high temperature *in-situ* reduction process. First, uniform Fe_3O_4 nanoparticles were prepared *via* a modified solvothermal process and then encapsulated with a resorcinol formaldehyde (RF) polymer layer through a sol-gel method, giving rise to core-shell structured Fe_3O_4@RF composites. Then, a biphase stratification method was adopted to coat CTAB/SiO_2 composite layer onto the surface of Fe_3O_4@C composites, which leads to Fe_3O_4@C@CTAB/SiO_2 composites. Finally, uniform yolk-shell structured Fe@void@$mSiO_2$ composites were obtained after calcination in N_2 at 850 °C.

TEM image (Fig. 2a) possesses that the hydrothermally synthesized Fe_3O_4 nanoparticles display well-dispersed morphology with a uniform particle size of ~120 nm. After the polymerization, a thin RF polymer layer of ~30 nm was successfully wrapped on the Fe_3O_4 nanoparticles (Fig. 2b). After deposition of a layer of mesoporous silica through the oil-water biphase stratification method, Fe_3O_4@C@CTAB/SiO_2 composites with discrete and regular spherical morphology can be formed (Fig. 2c).

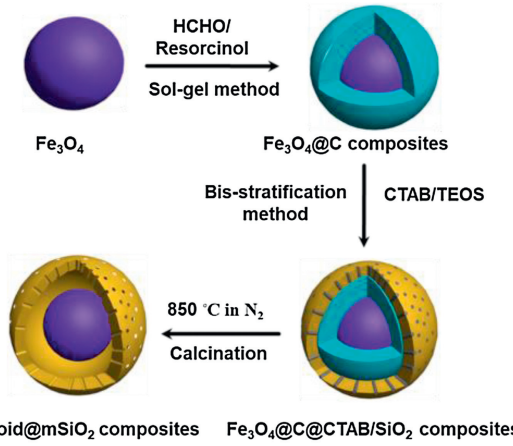

Fig. 1. Illustration of the formation of yolk-shell structured Fe@void@$mSiO_2$ composites.

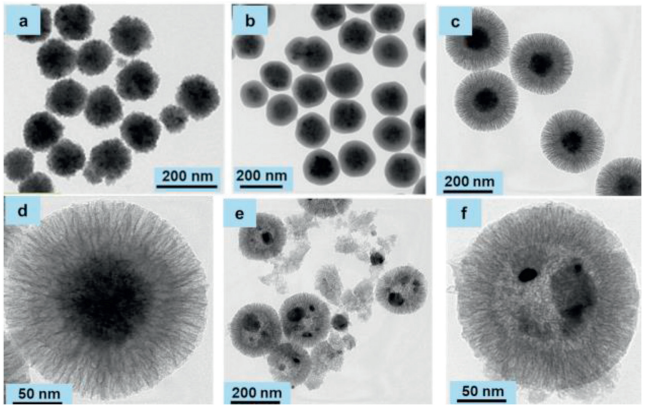

Fig. 2. TEM images of Fe_3O_4 (a), Fe_3O_4@C (b), Fe_3O_4@C@CTAB/SiO_2 (c, d) and Fe@void@mSiO_2 (e, f).

TEM images show that the Fe_3O_4@C@CTAB/SiO_2 composites possess a well-defined core-shell-shell structure with a layer of mesoporous silica in 40 nm thickness (Fig. 2d). After the *in-situ* high temperature reduction process, the well-defined core-shell structure was transformed to yolk-shell structure (Figs. 2e and f) with a number of nanoparticles broken, which is probably due to the recrystallization of Fe.

The wide-angle X-ray diffraction (XRD) pattern of Fe@void@m-SiO_2 composites (Fig. 3a) displayed several sharp which can be assigned to iron nanoparticles while they were not observed in Fe_3O_4. The wide peaks at 2θ = 22° and 26° can be assigned to amorphous mesoporous silica and the graphitized carbon, respectively. Two broad peaks located at 1350 and 1590 cm^{-1} in the Raman spectra are attributed to the D- and G- bands, respectively (Fig. 3b). The hysteresis loop data suggests that our material possess a quite high magnetization of 105 emu/g, which is much stronger than Fe_3O_4 (56 emu/g, Fig. 3c). Nitrogen adsorption-desorption isothermals show a typical type-IV curve with distinct hysteresis loops within the relative pressure band of 0.45-0.80, indicating the uniform mesoporous structure (Fig. 3d). The BET surface area of the Fe@void@mSiO_2 composites are calculated to be 495 m^2/g. The pore size distribution derived from the adsorption branch using the BJH method shows that the corresponding pore size is centered at 6.9 nm, making them an ideal candidate for the later applications.

The performance of the resultant magnetic mesoporous silica on the activation of PMS for the degradation of TC was examined at pH of 7 (Fig. 4a). As a comparison, the degradation performances of TC under PMS and ZVI were also examined, exhibiting the removal efficiencies of 19% and 39%, respectively in 60 min. When Fe@void@mSiO_2 nanospheres were used as the catalyst, the removal efficiency reaches to 100% in 40 min, clearly demonstrating the priority of Fe@void@mSiO_2 nanospheres. The effect of pH on the degradation performance of Fe@void@mSiO_2 (Fig. 4b) was

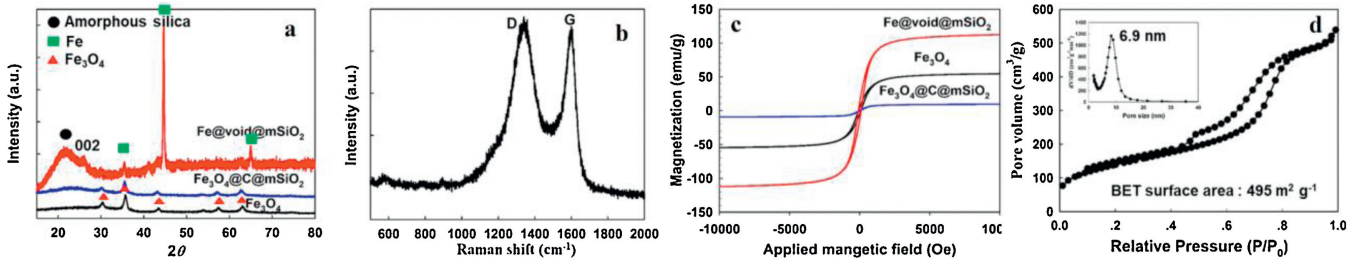

Fig. 3. (a) XRD patterns, (b) Raman spectra, (c) the magnetic hysteresis loops and (d) N_2 Sorption isotherms of the resultant materials.

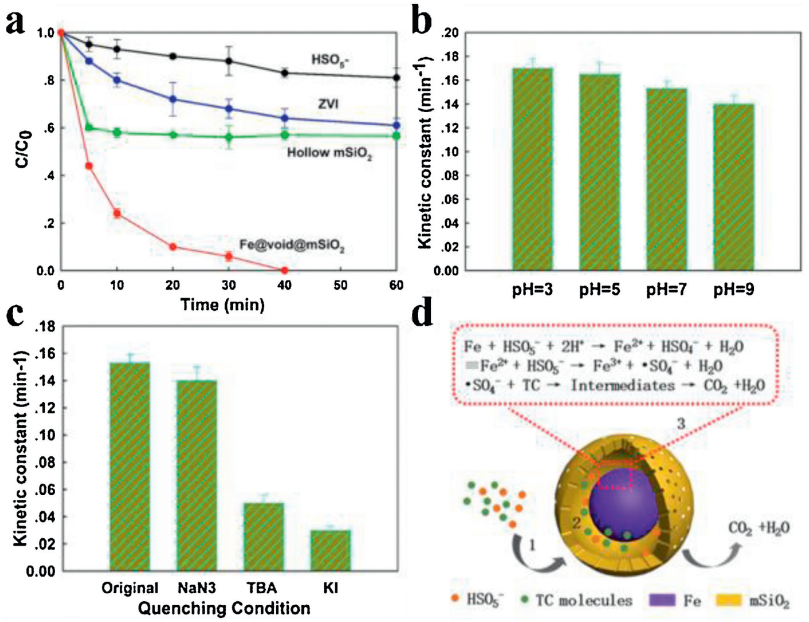

Fig. 4. (a) Degradation profile of different catalysts and (b) kinetic constants values at different pH. Experimental conditions: solution volume: 100 mL, catalyst dose: 0.1 g/L, PMS concentration: 0.18 g/L, T: 20 °C, initial TC concentration: 10 mg/L. (c) Scavenging test and (d) schematic illustration of the possible degradation mechanism.

investigated. In order to estimate the kinetic constant, a *pseudo*-first-order kinetic model was employed (Eq. 1).

$$\ln(\frac{C}{C_0}) = -kt \quad (1)$$

where C is the concentration of TC at time t, C_0 is the initial TC concentration and k is the *pseudo*-first-order reaction rate constant. We caught sight of the kinetic constant at pH of 7 and 9 are calculated to be 0.15 and 0.14 min^{-1}, respectively, slightly smaller than that at pH of 3, suggesting that such catalysts are able to work over a broad pH range. As illustrated in Fig. 4c, the production of $^{\bullet}OH/SO_4^{\bullet-}$ as the dominate species in this system was proved through the scavenging test. The addition of NaN_3 (singlet oxygen ($^1O_2$) scavenger) slightly reduced the reaction rate, indicating that $^1O_2$ is not the main species while the addition of tert-butanol significantly reduced the degradation rate, suggesting that $^{\bullet}OH/SO_4^{\bullet-}$ are the main contributor. Note that by the addition of KI, which is a scavenger for the surface bonded radicals, the reaction rate sharply reduced, suggesting that surface radicals play the most important role in the degradation process. Magnetic mesoporous silica exhibits extraordinary performance, which can be ascribed to the synergistic effect from its unique textual structures. Firstly, the ordered large mesopores facilitates the mass transfer of both PMS and TC molecules between solid and phases aqueous. Secondly, the presence of mesoporous silica shell greatly enhances the adsorption of pollutants molecules and enrichs them in the void space of the nanoreactor, which could be beneficial for surface reaction [44]. The adsorption test obviously shows that the hollow structured mesoporous silica shell possesses a high removal efficiency for TC (~40%). Finally, the surface iron species reacts with the adsorbed PMS to produce large quantity of radicals such as $^{\bullet}OH/SO_4^{\bullet-}$, which can directly *in-situ* oxidize the TC molecules confined in the void space into small molecules or even CO_2 and H_2O (Fig. 4d).

In summary, a successive coating strategy followed by a subsequent high-temperature *in-situ* treatment have been employed for the preparation of yolk-shell structured Fe@void@m-SiO_2 composites. The obtained composites exhibit a uniform pore size (~6.9 nm), a high specific surface area (~495.0 m^2/g) and a super large magnetic susceptibility (~105 emu/g), which is suitable for the activation of PMS to degrade organic pollutants. Compared with commercial ZVI nanoparticles, the composite catalyst possesses much more excellent degradation activity for tetracycline (TC) in a wide pH range and rapid recovery *via* using an external magnetic field. This study paves a new strategy to the diversification of catalysts for the Fenton-like process.

Declaration of competing interests

The authors declare that they have no known competing financial interests or personal relationships that could have appeared to influence the work reported in this paper.

Acknowledgments

This research is supported by the NSF of China (Nos. 51822202 and 51772050), Shanghai Rising-Star Program (No. 18QA1400100), Youth Top-notch Talent Support Program of Shanghai, Science and Technology Commission of Shanghai Municipality (No. 19520713200), Shanghai Scientific and Technological Innovation Project (No. 19JC1410400), DHU Distinguished Young Professor Program and Fundamental Research Funds for the Central Universities.

References

[1] X. Wen, Z. Zeng, C. Du, et al., Chemosphere 222 (2019) 865–871.
[2] J. Cao, Z. Xiong, B. Lai, Chem. Eng. J. 343 (2018) 492–499.
[3] J. Hu, R. Yang, Z. Li, et al., Solid State Sci. 92 (2019) 60–67.
[4] J.X. Fan, M.Y. Peng, H. Wang, et al., Adv. Mater. 31 (2019) 1808278.
[5] S. Navalon, R. Martin, M. Alvaro, H. Garcia, Angew. Chem. Int. Ed. 49 (2010) 8403–8407.
[6] D.Q. He, L.F. Wang, H. Jiang, H.Q. Yu, Chem. Eng. J. 272 (2015) 28–134.
[7] C. Hu, D. Huang, G. Zeng, et al., Chem. Eng. J. 338 (2018) 432–439.
[8] M. Cheng, G. Zeng, D. Huang, et al., J. Hazard. Mater. 312 (2016) 184–191.
[9] X. Yang, X. Cheng, A.A. Elzatahry, et al., Chin. Chem. Lett. 30 (2019) 324–330.
[10] L. Chen, J. Ma, X. Li, et al., Environ. Sci. Technol. 45 (2011) 3925–3930.
[11] G.P. Anipsitakis, D.D. Dionysiou, Environ. Sci. Technol. 37 (2003) 4790–4797.
[12] X. Li, X. Huang, S. Xi, et al., J. Am. Chem. Soc. 140 (2018) 12469–12475.
[13] X. Yang, X. Xu, J. Xu, Y. Han, J. Am. Chem. Soc. 135 (2013) 16058–16061.
[14] W.D. Oh, Z. Dong, T.T. Lim, Appl. Catal. B 194 (2016) 169–201.
[15] W.D. Oh, Z. Dong, G. Ronn, T.T. Lim, J. Hazard. Mater. 325 (2017) 71–81.
[16] Y. Wang, H. Sun, X. Duan, et al., Appl. Catal. B 172–173 (2015) 73–81.
[17] H. Sun, Y. Wang, S. Liu, et al., Chem. Commun. 49 (2013) 9914–9916.
[18] H. Sun, S. Liu, G. Zhou, et al., ACS Appl. Mater. Interfaces 4 (2012) 5466–5471.
[19] Y. Yang, Y. Tang, S. Liang, et al., Nano Energy 61 (2019) 617–625.
[20] H. Li, Q. Gao, H. Wang, et al., ACS Omega 3 (2018) 17724–17731.
[21] C.X. Zhao, B.Q. Li, J.N. Liu, J.Q. Huang, Q. Zhang, Chin. Chem. Lett. 30 (2019) 911–914.
[22] J. Liu, S.Z. Qiao, J.S. Chen, et al., Chem. Commun. 47 (2011) 12578–12591.
[23] Y. Chen, H. Chen, D. Zeng, et al., ACS Nano 10 (2010) 6001–6013.
[24] Z.M. Cui, Z. Chen, C.Y. Cao, L. Jiang, W.G. Song, Chem. Commun. 49 (2013) 2332–2334.
[25] C. Liu, J. Li, J. Qi, et al., ACS Appl. Mater. Interfaces 6 (2014) 13167–13173.
[26] T. Zhao, Y. Ren, G. Jia, et al., Chin. Chem. Lett. 30 (2019) 2032–2038.
[27] T. Zhu, L. Zhu, J. Wang, G.W. Ho, ACS Appl. Mater. Interfaces 8 (2016) 32901–32909.
[28] Z. Wu, K. Yu, S. Zhang, Y. Xie, J. Phys. Chem. C 112 (2008) 11307–11313.
[29] P. Rai, J.W. Yoon, H.M. Jeong, et al., Nanoscale 6 (2014) 8292–8299.
[30] J. Liu, H.Q. Yang, F. Kleitz, et al., Adv. Funct. Mater. 22 (2012) 591–599.
[31] Y. Boyjoo, K. Merigot, J.F. Lamonier, et al., RSC Adv. 5 (2015) 24872–24876.
[32] L. Yin, S. Song, X. Wang, et al., Environ. Pollut. 238 (2018) 725–738.
[33] P. Qiu, K. Kang, K. Kim, et al., RSC Adv. 5 (2015) 96201–96204.
[34] W. Li, D. Zhao, Adv. Mater. 25 (2013) 142–149.
[35] T. Yao, T. Cui, X. Fang, et al., Nanoscale 5 (2013) 5896–5904.
[36] K.A. Kuttiyiel, Y.M. Choi, K. Sasaki, et al., Nano Energy 29 (2016) 261–267.
[37] K.A. Kuttiyiel, Y.M. Choi, S.M. Hwang, et al., Nano Energy 13 (2015) 442–449.
[38] J. Liu, Z. Sun, Y. Deng, et al., Angew. Chem. Int. Ed. 48 (2009) 5875–5879.
[39] B. Thokchom, P. Qiu, M. Cui, et al., Ultrason. Sonochem. 34 (2017) 262–272.
[40] Z. Sun, Q. Yue, Y. Liu, et al., J. Mater. Chem. A 2 (2014) 18322–18328.
[41] X. Fang, C. Chen, Z. Liu, P. Liu, N. Zheng, Nanoscale 3 (2011) 1632–1639.
[42] Y.Y. Pu, Y. Li, W. Zhuang, et al., Chin. Chem. Lett. 23 (2012) 1201–1204.
[43] W. Li, Y. Deng, Z. Wu, et al., J. Am. Chem. Soc. 133 (2011) 15830–15833.
[44] J. Liu, J. Cheng, R. Che, et al., ACS Appl. Mater. Interfaces 5 (2013) 2503–2509.